Selective Hydrogenation of Furfural in a Proton Exchange Membrane Reactor Using Hybrid Pd/Pd Black on Alumina

Sarah Carl,[a] Krysta Waldrop,[b] Peter Pintauro,[b] Levi T. Thompson,[a, c] and William A. Tarpeh*[d]

Conventional thermocatalytic hydrogenation employs high temperatures and pressures and often exhibits low selectivity toward desired products. Electrochemical hydrogenation can reduce energy input by operating at ambient conditions and improving process control and selectivity; however, electrocatalysts face stability and conductivity limitations. To overcome these obstacles, we physically mixed a traditional electrocatalyst (Pd black) with a hydrogenation-active metal (Pd) supported on a conventional metal oxide support (alumina, Al_2O_3) and investigated electrochemical hydrogenation of furfural, a model biomass compound. Experiments were conducted in a proton exchange membrane (PEM) reactor, in which synthesized electrocatalysts were used as cathodes. Catalysts with Pd black and varying loadings of Pd on Al_2O_3 were used to determine the impact of hydrogen spillover on electrocatalytic hydrogenation mechanisms, selectivity, and rates. Observed hydrogenation rates and selectivities were linked to structural and compositional properties of the catalyst mixtures. Of the Pd black cathodes tested, 5 wt% Pd/Al_2O_3 exhibited production rates as high as pure Pd black and higher selectivity towards completely hydrogenated products. Improved selectivity and rates were attributed to a synergistic interaction between Pd black and 5 wt% Pd/Al_2O_3 in which Pd/Al_2O_3 increased the number of active sites, while Pd black provided stable conductivity.

1. Introduction

Selective hydrogenation is an important class of catalytic reactions used to synthesize various products, including perfumes, organic intermediates, and pharmaceuticals.[1–4] Industrially, these reactions are typically conducted thermochemically at high temperatures (up to 425 °C) and pressures (up to 130 bar) to overcome the low hydrogen solubility in liquid systems[5–9] and the kinetic barrier of thermal H_2 splitting.[8,10–12] Electrochemical reduction, specifically electrocatalytic hydrogenation, can overcome hydrogen solubility and avoid thermal H_2 splitting while operating at atmospheric pressure and lower temperatures.[8,12–17]

In addition to operating at more mild conditions, electrochemical hydrogenation exhibits several advantages over thermocatalytic approaches. Electrochemical hydrogen production can be directly controlled by current density, facilitating more efficient use of hydrogen for hydrogenation.[12,18,19] Electrochemical hydrogenation has been demonstrated for multiple industrial reactions (e.g., nitrobenzene to azobenzene, naphthalene to 1,4-dihydronaphthalene[20,21]) and can improve selectivity and rate over thermochemical hydrogenation.[8,9,12,16–18,22–29] Additionally, electrochemical processes can exhibit fewer environmental impacts than thermochemical processes by utilizing electricity generated from renewable energy resources. As of 2017, 80% of energy consumed by U.S. industrial production comes from petroleum, natural gas, and coal—all of which emit a total of 964 million metric tons of carbon dioxide annually.[30,31] By enabling hydrogenation powered by renewable energy, electrochemical hydrogenation can reduce greenhouse gas emissions and accelerate process intensification.

Despite its potential benefits, electrocatalytic hydrogenation has been limited by the slow development of stable electrocatalysts for which hydrogen evolution does not predominate over hydrogenation.[10,12,17] An ideal electrocatalyst would exhibit selectivity toward hydrogenation over hydrogen evolution, high conductivity, and stability at extreme pH values and high overpotentials.[32–35] Currently, the most commonly studied electrocatalysts are noble metals loaded onto carbon (e.g., Pd/C or Pt/C) aimed at improving stability compared to either material separately.[35–39] To combat stability limitations and expand the range of potential electrocatalysts, we investigated a hybrid cathode that is a physical mixture of an electrocatalyst and a metal loaded onto a conventional metal oxide support (in this case alumina, Al_2O_3), in a proton exchange membrane (PEM) reactor. The idea of this mixed cathode was derived from our previous work that demonstrated an improvement in

[a] S. Carl, Dr. L. T. Thompson
     Department of Chemical Engineering
     University of Michigan
     Ann Arbor, MI 48105, USA
[b] K. Waldrop, Dr. P. Pintauro
     Department of Chemical and Biomolecular Engineering
     Vanderbilt University
     Nashville, TN 37240, USA
[c] Dr. L. T. Thompson
     Department of Chemical and Biomolecular Engineering
     University of Delaware
     Newark, DE, 19717 USA
[d] Dr. W. A. Tarpeh
     Department of Chemical Engineering
     Stanford University
     Stanford, CA, 94305, USA
     E-mail: wtarpeh@stanford.edu

triglyceride hydrogenation rate due to the synergistic interaction between the Pd metal and tungsten carbide (W_2C) support compared to those of Pd alone and W_2C alone.[40] Similarly, the hybrid Pd black with Pd/Al_2O_3 cathode in this study may exhibit advantages of both electrocatalysts and thermocatalysts. The electrocatalyst may provide in situ surface-bound hydrogen and generation of hydrogen, while the metal loaded on Al_2O_3 may utilize hydrogen spillover from the electrocatalyst for hydrogenation.

Furfural, a well-studied indicator compound for biomass, was chosen as the probe molecule to evaluate the performance of the hybrid cathode.[23,41–52] Commonly reported reaction pathways include either hydrogenation, hydrodeoxygenation, or decarbonylation followed by hydrogenation of the furan ring (Figure 1). The tendency towards decarbonylation or hydrogenation depends on the availability of hydrogen near the Pd surface. A recent study used density functional theory to show that furan (decarbonylation product) forms under low hydrogen coverage but furfuryl alcohol (hydrogenation product) forms at high hydrogen coverage.[43] Experimental studies supported these computational results by demonstrating that the selectivity for furan shifted to furfuryl alcohol at increased H_2 pressure.[41,53,54] Hydrogen coverage also affects relative selectivity toward hydrodeoxygenation over hydrogenation. Under H_2-rich conditions, Cu/SiO_2 yields higher selectivity for furfuryl alcohol at lower temperatures and for 2-methylfuran at higher temperatures due to the proposed Eley-Rideal mechanism. This mechanism exhibits a rate-determining step of water removal from the surface, which inhibits the intermediate from dissociating into 2-methylfuran.[41,55] With these distinctions in reaction pathways for furfural, the catalyst performance could be understood by correlating the hydrogen coverage on the surface to selectivity and hydrogenation rate.

In this study, the performance of different cathode compositions was evaluated at different current densities (which vary with hydrogen production) in terms of production rate, faradaic efficiency, and selectivity. To isolate the influences of the electrocatalyst in the hybrid catalyst, the performance of electrocatalyst Pd black (Pd_{black}) was evaluated separately. These four variations of the hybrid cathode - Pd_{black} with alumina (Al_2O_3), Pd_{black} with 2.7 wt% Pd/Al_2O_3, Pd_{black} with 5 wt% Pd/Al_2O_3, and Pd_{black} with 50 wt% Pd/Al_2O_3 - were investigated to test the hypothesis that the addition of the metal loaded on metal oxide to the electrocatalyst enhances the production rate for hydrogenated products compared to electrodes with only an electrocatalyst. Each variation of hybrid cathode was compared to the Pd_{black}-only cathode to determine how the alumina influenced the activity of Pd_{black} via production rate, faradaic efficiency, and carbon selectivity.

Experimental Section

Catalysis Synthesis and Membrane Electrode Assembly

The Pd loaded on Al_2O_3 was synthesized via dry impregnation. First, the Al_2O_3 (Sigma Aldrich) was pressed and sieved to retain 125–250 μm particles, and calcined in air at 500 °C. To load Pd, the desired amount of metal precursor (Pd(NO_3)$_2$•H_2O, Sigma Aldrich) was dissolved in a volume of ultrapure water equal to the support pore volume, as determined by N_2 adsorption measurements and Brunauer, Emmett, and Teller (BET) calculations using Micromeritics ASAP 2010. To achieve uniform dispersion, the solution containing metal precursor was added dropwise to the support and mixed thoroughly. The preloaded support with the metal precursor was dried in a vacuum oven overnight before being calcined and reduced at 300 °C in 5% H_2/Ar. Catalysts were characterized by X-ray diffraction (XRD) and N_2 adsorption to determine the bulk phase and surface area using BET calculations, respectively. To examine the surface of the catalyst after conducting a reaction, scanning electron microscopy (SEM) with energy dispersive spectroscopy (EDS) was conducted on membrane electrode assemblies (MEAs) exposed to constant current densities.

For the electrocatalyst, Pd_{black} (Sigma-Aldrich) was purchased and used without additional modification and physically mixed with the conventional catalyst during the creation of the electrode ink. The anode catalyst, 40% Pt/C, was also used as purchased and kept constant for all MEAs fabricated.

For the electrode ink, the alumina-containing cathode was sonicated for 30 minutes with water to ensure sufficient catalyst wetting. 20 wt% Nafion stock solution (in water:alcohol) and alcohol were added to the mixture before being sonicated and mechanically mixed for another 30 minutes. Afterward, sufficient Pd_{black} was added to the cathode ink to ensure conductivity across the cathode as dictated by percolation theory. The resultant inks were mechanically mixed overnight and painted onto a 5 cm^2 Sigracet 29 BC gas diffusion layer (IonPower). All inks had a solid content of 10 wt%. The final anode composition was 80:20 wt% Pt/C: Nafion with a Pt loading of 2.0 ± 0.1 mg/cm^2. The final cathode composition was 54:26:20 wt% catalyst: Pd_{black}: Nafion with a catalyst loading of 2.0 ± 0.1 mg/cm^2. The anode and cathode gas diffusion electrodes were placed onto either side of a Nafion 212 membrane and hot-pressed at 140 °C and 5 MPa for 5 minutes. MEA thickness was measured with calipers and used for calculating proton conductivity.

Electrocatalytic Experiments

Vapor phase electrochemical experiments were conducted in a single-pass PEM reactor consisting of anode and cathode graphite blocks separated by a selective membrane for proton transport, which reduces mass transport limitations compared to conventional H-cell experiments (Figure 2).[32,56] Both graphite blocks have a serpentine flow field. Humidified hydrogen flowed at ~130 mL/min on the anode side, while argon flowed at ~55 mL/min through
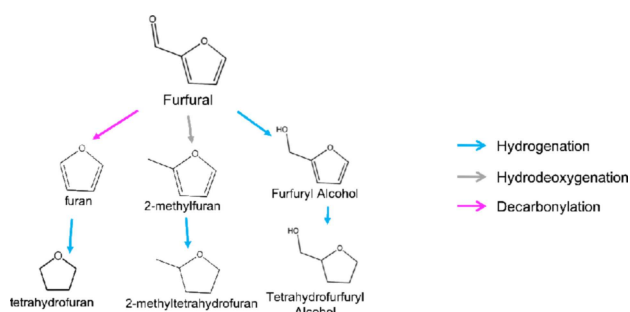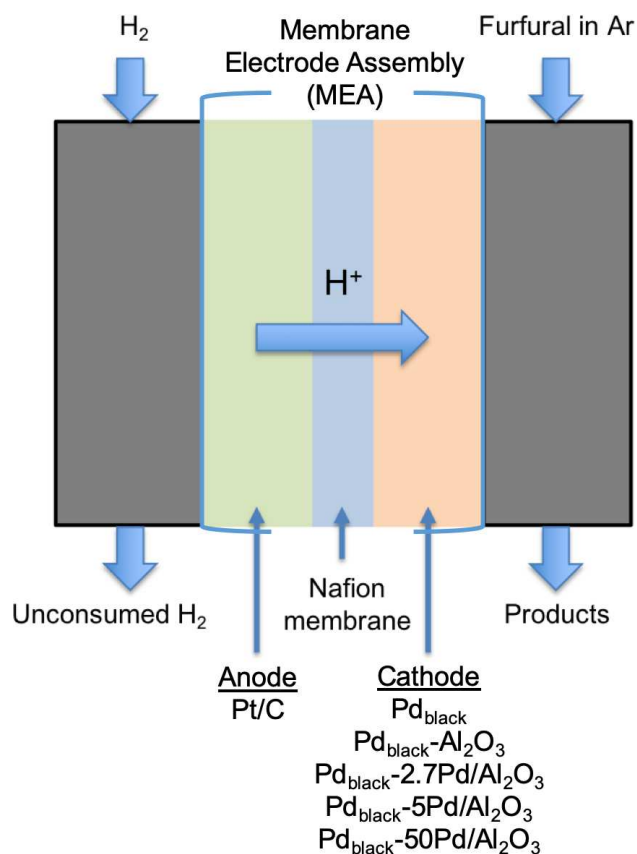

Figure 1. Reaction pathways evaluated for furfural consists of hydrogenation (blue arrows), hydrodeoxygenation (orange arrows), and decarbonylation (black arrows).

Figure 2. Diagram of a proton exchange membrane reactor with a membrane electrode assembly (MEA) inserted in the middle. The anode has H_2 flowing over Pt/C, while the cathode has furfural in Ar flowing over the tested catalysts. The membrane of the MEA is Nafion.

bubblers containing furfural (99%, Sigma Aldrich) in a room temperature water bath on the cathode side (~0.2 μmol/s of furfural). The products were analyzed via in-line gas chromatography with a flame ionization detector (GC-FID). The PEM reactor was maintained at 80 °C, and the lines to the PEM reactor and to the GC-FID were heated to retain reactants and products in vapor phase. Constant current densities (10 mA/cm² and 50 mA/cm²) were applied via potentiostat (Autolab PGSTAT302 N) with the cathode as the working electrode and the anode as the counter electrode for 9 hours to yield relatively stable production rates (±5% in voltage). The presented results are averages over the last 8 hours. Based on preliminary experiments, 10 mA/cm² and 50 mA/cm² were chosen as values representing, respectively, low and high regions of proton delivery (discussed in detail in SI and shown in Figure S1). A new MEA was utilized for every experiment to exclude potential effects from previous experiments.

Cyclic voltammetry (CV) and electrochemical impedance spectroscopy (EIS) were performed before and after each constant current density experiment to verify MEA activity and resistance, respectively. Without furfural, CV was used to evaluate MEA activity for hydrogen adsorption and desorption. For CV, the open circuit potential (OCP) was measured after stabilization (±1 mV) and taken as the starting voltage without furfural present. 20 cycles were monitored at a scan rate of 20 mV/s with a sweep from 24 mV to 650 mV at a step voltage of 1 mV. The last cycle measured was used to compare CVs taken before and after each experiment. EIS was performed with and without furfural present to evaluate MEA resistance. The OCP was measured after stabilization before starting

the sweep of frequencies from 100 kHz to 0.01 Hz. Nyquist plots were utilized to determine the resistance of solution in the MEA (example shown in Figure S2). EIS performed in the presence of furfural was used to understand how the proton conductivity of the cathode changes when the insulating material is added. The proton conductivity (σ) can be determined using Equation (1):

$$\sigma = \frac{L}{Z'S} \tag{1}$$

in which Z' denotes the real impedance at the highest frequency, L is the thickness of the electrode, and S is the area of the electrode.[32]

For each experiment, we evaluated catalyst performance by determining total production rate (of all furfural products), carbon selectivity, and faradaic efficiency. The total production rate of the carbonaceous compounds indicates how reactive the catalyst is to furfural and is quantified using the GC-FID. Carbon selectivity, which specifies the reaction pathway of furfural, was determined for each product by dividing the production rate of each product by the total production rate determined by the GC-FID. The proportion of electrons used for furfural hydrogenation was quantified as the faradaic efficiency (FE) using Equation (2), in which x_i is the mole fraction of product i (unitless), n is the number of moles of electrons required for reducing furfural to product i (mol), Q is the volumetric flow rate (cm³/min), F is Faraday's constant (C/mol), and I is the recorded current (A).

$$FE_i \, (\%) = \frac{x_i \, n \, Q \, F}{I} \tag{2}$$

CO Adsorption Experiment

Because Pd is known to readily absorb H_2, the H_2 pulse adsorption experiment may inaccurately determine the number of active sites.[57] Knowing the accurate number of active sites is vital when comparing different catalysts in terms of production rate and selectivity. To address this challenge, we used CO pulse adsorption to determine the number of active sites for each catalyst using the AutoChem II 2920.[58–60] For each test, ~200 mg of catalyst was heated to 450 °C for 1 hour to clean the surface; subsequently, the temperature was lowered to 30 °C. CO titration was performed via pulse adsorption of 5% CO/He until saturation. The ratio of CO:Pd was assumed to be 1:1 when calculating the active sites and dispersion.[60]

2. Results and Discussion

2.1. Properties of Cathode Catalysts

Table 1 lists the cathode catalysts used and their physical properties prior to incorporating them into a membrane electrode assembly (MEA). The bulk Pd_{black} has notably lower surface area than any catalyst containing Al_2O_3; the surface area of the Al_2O_3 decreased with increasing amounts of Pd, indicating that pores increasingly filled with Pd. The Pd particle size and active sites were obtained using CO pulse chemisorption; the Pd_{black} exhibited significantly larger particle size and fewer active sites compared to any Pd/Al_2O_3. XRD demonstrated

Table 1. Physical properties of cathode catalysts.

Catalyst	Pd weight percent [%]	Surface area [m^2/g]	Pd on Al$_2$O$_3$ [mg/cm^2]	Monolayer Pd coverage on Al$_2$O$_3$ [%][a]	Pd active sites [10^{20} atoms/g$_{Pd}$][b]	Pd particle size [nm][c]
Pd$_{black}$	–	15.6	–	–	0.092	721
Al$_2$O$_3$	–	88.0	–	–	–	–
2.7 wt% Pd/Al$_2$O$_3$	2.7	66.1	0.05	20	17.4	3.8
5 wt% Pd/Al$_2$O$_3$	5	68.0	0.1	33	10.8	6.2
50 wt% Pd/Al$_2$O$_3$	50	46.0	1	333	3.01	22

[a] Calculated by using the surface area and amount of metals in the catalyst. [b] Calculated by multiplying the amount of CO absorbed on Pd with the Avogadro's number. [c] The Pd particles were assumed to be spherical.

that all catalysts retain a similar Pd crystalline structure (Figure S3).

The different compositions of cathodes tested were 1 mg/cm^2 Pd$_{black}$ (denoted as Pd$_{black}$), 1 mg/cm^2 Pd$_{black}$ physically mixed with 2 mg/cm^2 bare Al$_2$O$_3$ (Pd$_{black}$-Al$_2$O$_3$), and 1 mg/cm^2 Pd$_{black}$ physically mixed with 2 mg/cm^2 of different Pd loadings on Al$_2$O$_3$. The denotation for these Pd/Al$_2$O$_3$ containing cathodes is Pd$_{black}$-yPd/Al$_2$O$_3$ in which the "y" represents the Pd weight loading; for example, 2.7 wt% Pd/Al$_2$O$_3$ physically mixed with Pd$_{black}$ is denoted as Pd$_{black}$-2.7Pd/Al$_2$O$_3$. At the OCP, the proton conductivity for all cathodes was uniformly (within error) 0.04 ± 0.01 S/cm, indicating that similar proton conductivity can be achieved even with varying catalyst layer thickness and cathode composition.

In addition to providing information on the proton conductivity, EIS provided insight on the charge transfer resistance of electrons between the electrode and the adsorbed species. The charge transfer resistance for Pd$_{black}$-Al$_2$O$_3$ was an order of magnitude higher (64.0 Ω) than that for Pd$_{black}$ (7.7 Ω). Although both cathode materials had similar amounts of Pd$_{black}$, the addition of insulating alumina appears to have increased the amount of energy required for electrons to transfer from the cathode to adsorbed species such as hydrogen and furfural. For Pd$_{black}$-Al$_2$O$_3$ variations, charge transfer resistance generally decreased with Pd loading, except for Pd$_{black}$-2.7Pd/Al$_2$O$_3$ (Figure S4). The difference for Pd$_{black}$-2.7Pd/Al$_2$O$_3$ may be attributed to how furfural interacts with the active sites as the charge transfer resistance without furfural present was 2.8 Ω, which is a similar magnitude to Pd$_{black}$-Al$_2$O$_3$ (9 Ω). While the proton conductivity for each material was similar, the difference in charge transfer resistance indicated the movement of electrons through the carbon paper to the metal particles varies with cathode composition. Thus, the dispersion of Pd particles did not impact proton conductivity but did influence electronic conductivity. This difference in charge transfer may influence the production rate or selectivity for the cathodes.

2.2. Total Production Rate and Sum of Faradaic Efficiency

The total carbonaceous production rates and faradaic efficiencies for Pd$_{black}$, Pd$_{black}$-Al$_2$O$_3$, Pd$_{black}$-2.7Pd/Al$_2$O$_3$, Pd$_{black}$-5Pd/Al$_2$O$_3$, and Pd$_{black}$-50Pd/Al$_2$O$_3$ cathodes are shown in Figure 3 at 10 mA/cm^2 and 50 mA/cm^2.
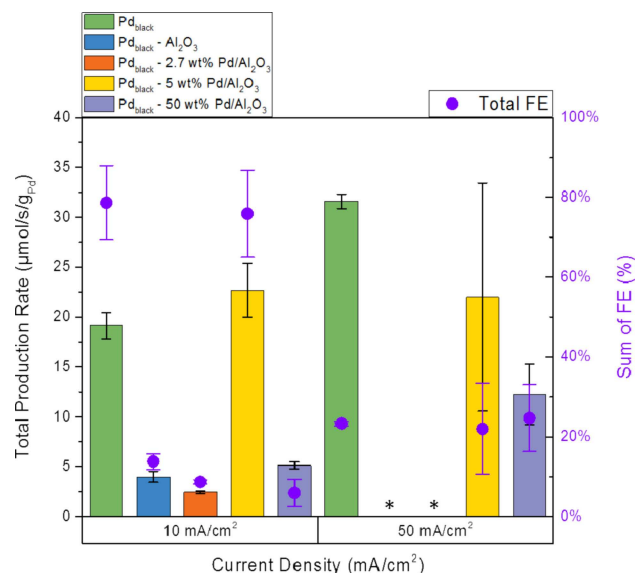

Figure 3. Total production rates (left y-axis) and sum of carbonaceous faradaic efficiencies (right y-axis) at 10 mA/cm^2 and 50 mA/cm^2 for Pd$_{black}$ (green bars), Pd$_{black}$-Pd/Al$_2$O$_3$ (blue bars), Pd$_{black}$-2.7Pd/Al$_2$O$_3$ (orange bars), Pd$_{black}$-5Pd/Al$_2$O$_3$ (yellow bars), and Pd$_{black}$-50Pd/Al$_2$O$_3$ (purple bars). The "*" symbol indicates that the current density applied was not achieved.

At 10 mA/cm^2, Pd$_{black}$-Al$_2$O$_3$ exhibited notably lower production rate and faradaic efficiency than Pd$_{black}$, even though Pd$_{black}$-Al$_2$O$_3$ had the same amount of Pd$_{black}$ and similar proton conductivity. This difference may be attributed to the higher charge transfer resistance of Pd$_{black}$-Al$_2$O$_3$, causing insufficient electrons to complete the electrochemical reaction with the proton and furfural. Among variations of Pd/Al$_2$O$_3$ loading, the 5 wt% yielded higher activity than both the 2.7 wt% and 50 wt%, indicating an optimal loading for the Pd/Al$_2$O$_3$. Potentials measured with respect to the quasi hydrogen electrode reference decreased with increasing Pd loading (Figure S5); Pd$_{black}$ had a much lower voltage of 119 mV than Pd$_{black}$-5Pd/Al$_2$O$_3$ at 360 mV, even though the performance and conversions were similar (65% ± 5%). This discrepancy demonstrated that potential did not correlate with production rate or faradaic efficiency; instead, potentials highlight the importance of the electronic conductivity for production rate and faradaic efficiency.

At 50 mA/cm^2, the relationships between total production rates of cathode variations were similar to 10 mA/cm^2: Pd$_{black}$-

Table 2. Proton conductivity for all cathodes measured after 10 mA/cm² and 50 mA/cm².

Cathode	Pd_{black}	Pd_{black}-Al_2O_3	Pd_{black}-2.7Pd/Al_2O_3	Pd_{black}-5Pd/Al_2O_3	Pd_{black}-50Pd/Al_2O_3
Proton conductivity after 10 mA/cm² (10³ S/cm)	30 ± 5	20 ± 5	8 ± 1	20 ± 5	40 ± 5
Proton conductivity after 50 mA/cm² (10³ S/cm)	30 ± 5	0.3 ± 0.01	0.3 ± 0.01	2 ± 1	10 ± 5

5Pd/Al_2O_3 yielded similar activities to Pd_{black} and higher rates than both 2.7 wt% and 50 wt%. For these three cathode variations, the production rates at 50 mA/cm² were equal to or higher than those observed at 10 mA/cm² due to more protons driven to the electrode at the higher current density. In contrast, the Pd_{black}-Al_2O_3 and Pd_{black}-2.7Pd/Al_2O_3 could not achieve the set current density of 50 mA/cm² due to the potentiostat reaching its maximum operating voltage of 10 V. The faradaic efficiencies of the Pd_{black} and Pd_{black}-5Pd/Al_2O_3 at 50 mA/cm² were lower than those at 10 mA/cm² but still similar for the two materials. The lower faradaic efficiencies for these cathodes at 50 mA/cm² indicated a low proportion of electrons reacted with furfural; the remainder were most likely consumed by hydrogen evolution reaction. Only Pd_{black}-50Pd/Al_2O_3 exhibited an increase in faradaic efficiency, indicating increased utilization of the active material at higher current density. Similarly, the conversion for this catalyst also increased from 34% ± 3% to 50% ± 12%. Despite Pd_{black}-50Pd/Al_2O_3 having twice as much active material as the other cathodes, its lower production rate, conversion, and faradaic efficiency suggests that more active material does not improve activity because most of the active material is not utilized.

The stability for the different cathode variations increased with the increase in Pd loading on Al_2O_3. Both Pd_{black}-Al_2O_3 and Pd_{black}-2.7Pd/Al_2O_3 had the lowest rates and efficiencies at 10 mA/cm² and could not achieve 50 mA/cm² due to poor electrical conductivity. Similarly, these catalysts also had the lowest conversions within the range of 10% to 15%, reflecting their poor activity and conductivity. While Pd_{black}-5Pd/Al_2O_3 yielded similar activity to that of Pd_{black} at both current densities, it had large error bars at 50 mA/cm². The furfural conversion for Pd_{black} was stable around 40% ± 3%, while that for Pd_{black}-5Pd/Al_2O_3 was continuously decreasing from 80% to 20% at 50 mA/cm². These large error bars for production rate, conversion, and efficiency indicate that Pd_{black}-5Pd/Al_2O_3 suffered a decrease in activity as time progressed, indicating that this hybrid cathode is not stable at 50 mA/cm². The measured voltage with respect to the quasi hydrogen electrode reference also reflected the instability of the Pd_{black}-5Pd/Al_2O_3, as the voltage started at 662 mV and ended at 1.87 V, whereas the voltage for Pd_{black} remained relatively constant around 541 mV. The increase in current density improved the total production rate and faradaic efficiency for the Pd_{black}-50Pd/Al_2O_3 and may be attributed to the increased availability of hydrogen. This cathode had also retained stable activity unlike that of Pd_{black}-5Pd/Al_2O_3. Investigation of all cathodes at either current density of 10 mA/cm² or 50 mA/cm² using SEMS with EDS indicated that the difference in stability may be attributed to sintering (Figures S6 and S7). Because Pd_{black}-50Pd/Al_2O_3 had more active material than

Pd_{black}-5Pd/Al_2O_3, sintering did not impact its activity as drastically as it did for Pd_{black}-5Pd/Al_2O_3.

In general, the Pd_{black} cathode maintained its proton conductivity when current density was increased, while the hybrid cathodes experienced a loss in proton conductivity (Table 2). Among hybrid cathodes, the impact of applying a high current density was largest on the proton conductivity for the lowest Pd loading. Proton conductivity and charge transfer resistance appear to be key parameters that influence production rate and faradaic efficiency for these different cathode compositions. Due to the decrease in proton conductivity and the higher charge transfer resistance, the total production rate and faradaic efficiency for the hybrid cathodes appears to be severely hindered as the number of accessible active sites for electrochemical reaction decreased. This loss of activity is most notable at 50 mA/cm², in which Pd_{black}-5Pd/Al_2O_3 cannot maintain a constant production rate as the proton conductivity decreased by an order of magnitude at the end of the reaction. To maintain stable production rates, hybrid cathodes must balance between retaining constant proton conductivity and low charge transfer resistance during the reaction.

2.3. Carbon Selectivity

Although the total production rates for Pd_{black} and Pd_{black}-5Pd/Al_2O_3 were similar, the carbon selectivities exhibited notable differences (Figure 4). Understanding the influence of the
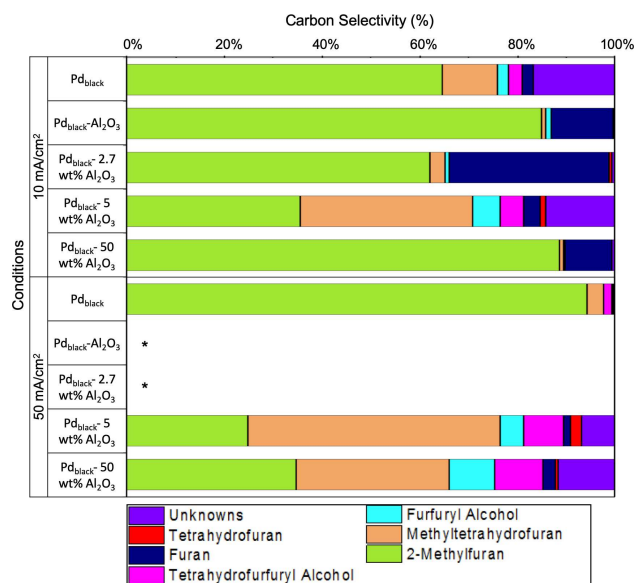
Figure 4. Carbon selectivities at 10 mA/cm² and 50 mA/cm² for Pd_{black}, Pd_{black}-2.7Pd/Al_2O_3, Pd_{black}-5Pd/Al_2O_3, and Pd_{black}-50Pd/Al_2O_3.

cathode composition on carbon selectivity provides insight on designing the cathode for improved control over selectivity. At 10 mA/cm^2, the selectivity for 2-methylfuran (MF) was dominant for all cathodes; however, notable differences in selectivity for other products on the hybrid catalysts were observed. Pd$_{black}$-5Pd/Al$_2$O$_3$ had the highest selectivity for the completely hydrogenated product of 2-methyltetrahydrofuran (MTHF) at 35%. Pd$_{black}$-Al$_2$O$_3$, Pd$_{black}$-2.7PdAl$_2$O$_3$, and Pd$_{black}$-50Pd/Al$_2$O$_3$ had high selectivity for furan, the decarbonylation product, than either those of Pd$_{black}$ and Pd$_{black}$-5Pd/Al$_2$O$_3$ at 10 mA/cm^2. Increasing the current density to 50 mA/cm^2 further highlighted the differences between these cathodes. For Pd$_{black}$, the hydrodeoxygenation product (MF) dominated the selectivity at 50 mA/cm^2; however, Pd$_{black}$-5Pd/Al$_2$O$_3$ cathode had preference for the completely hydrogenated product MTHF over MF. In addition to increasing its production rate and faradaic efficiency at the higher current density, the Pd$_{black}$-50Pd/Al$_2$O$_3$ cathode also increased production towards the hydrogenated products. This difference in carbon selectivity for the decarbonylation and hydrodeoxygenation pathways highlights the difference of how the molecules (furfural, H$_2$, intermediates, and furfural transformation products) interact with the surface.

The decarbonylation product is favored for Pd at low hydrogen coverage on the Pd surface whereas the hydrogenation product is favored at high hydrogen coverage.[43] The high selectivity for furan for the Pd$_{black}$-Al$_2$O$_3$ and Pd$_{black}$-2.7Pd/Al$_2$O$_3$ cathodes suggests a lack of hydrogen present in close proximity to furfural, supporting the speculation of loss of proton conductivity due to Pd particles agglomerating and decreasing active sites. While Pd$_{black}$-5Pd/Al$_2$O$_3$ proton conductivity also decreased after applying 10 mA/cm^2, it did not yield comparable selectivity for furan due to having more active sites present, permitting more hydrogen on the surface. Even at the higher current density of 50 mA/cm^2 with a significant decrease in proton conductivity, Pd$_{black}$-5Pd/Al$_2$O$_3$ had more active sites than either Pd$_{black}$-Al$_2$O$_3$ and Pd$_{black}$ (Table 1), allowing sufficient hydrogen coverage to hinder furan formation. The change in selectivity and rate for Pd$_{black}$-50Pd/Al$_2$O$_3$ differs from the other hybrid cathodes, as this cathode may not utilize all of its active sites. A 2 mg/cm^2 Pd$_{black}$ cathode was tested to compare with Pd$_{black}$-50Pd/Al$_2$O$_3$, because both cathodes have 2 mg/cm^2 Pd, and demonstrated that the 2 mg/cm^2 Pd$_{black}$ cathode yielded similarly lower production rates and efficiencies than 1 mg/cm^2 Pd$_{black}$ as well (shown in Figure S8). Thus, the higher influx of protons at the higher current density of 50 mA/cm^2 utilize more of the active material than at 10 mA/cm^2 as reflected with higher selectivity towards hydrogenated products. While the 50 wt% Pd/Al$_2$O$_3$ may provide more active sites, the loading of ~1 mg/cm^2 of Pd is optimal for efficient utilization of all of the active materials for hydrogenation.

Although furfuryl alcohol (FA) is the putative dominant product for gas phase hydrogenation, MF was typically the favored product in this study. This preference for hydrodeoxygenation instead of hydrogenation is attributed to the acidic environment provided by the Nafion membrane. Nafion is known to be a superacid when the membrane is hydrated due to the proton transport mechanism that utilizes its sulfonic acid groups. To support this speculation, an experiment without humidifying the anode stream was conducted with Pd$_{black}$ as the cathode. There was no conversion of furfural to MF, but there was conversion to FA without water present to humidify the membrane. Therefore, the strong acidity provided by humidified superacid Nafion membrane had a strong influence on the selectivity of furfural and could preferentially be used to generate 2-methylfuran.

Achieving sufficient hydrogen coverage for the higher number of active sites for Pd$_{black}$-5Pd/Al$_2$O$_3$ than Pd$_{black}$ at either current density may be attributed to the high charge transfer resistance of the 5% Pd cathode. Because the transfer of electrons from the electrode to the molecule is slower for Pd$_{black}$-5Pd/Al$_2$O$_3$ than Pd$_{black}$, the proton may stay near the surface longer, allowing for complete hydrogenation to MTHF. The increase in selectivity for MF observed with Pd$_{black}$ from 10 mA/cm^2 to 50 mA/cm^2 may be attributed to the retention of protons that are driven off the surface for hydrogen evolution faster due to the lower charge transfer resistance. The area of the hydrogen evolution peak from the CVs for Pd$_{black}$-5Pd/Al$_2$O$_3$ is smaller than that of Pd$_{black}$, indicating that hydrogen evolution is not as prevalent for the hybrid catalyst even though both cathodes have similar proton conductivities (Figure S9).

2.4. Turnover Frequency

The turnover frequencies (TOF) of Pd$_{black}$, Pd$_{black}$-5Pd/Al$_2$O$_3$, and Pd$_{black}$-50Pd/Al$_2$O$_3$ were compared and correlated with the selectivity for complete hydrogenation. Because MTHF and tetrahydrofurfuryl alcohol (THFA) are derived from the hydrogenation pathways and required the most H$_2$, these products may provide additional insight about hydrogen coverage on the catalyst surface. Figure 5 depicts the carbon selectivity of MTHF and THFA for each cathode and the logarithm of TOF plotted against catalyst type and current density.

The Pd$_{black}$-5Pd/Al$_2$O$_3$ cathode exhibited a low TOF with high selectivity towards completely hydrogenated products, while the Pd$_{black}$ electrode showed the inverse trend for TOF and selectivity. This trend suggests that a larger number of active sites promotes higher selectivity for completely hydrogenated products. Notably, Pd$_{black}$-50Pd/Al$_2$O$_3$ also yielded similar TOF to Pd$_{black}$-5Pd/Al$_2$O$_3$ but exhibited lower selectivity for completely hydrogenated products at 10 mA/cm^2, indicating that increasing the available number of active sites is not the only parameter that influences selectivity toward completely hydrogenated products. Because Pd$_{black}$-5Pd/Al$_2$O$_3$ has a higher charge transfer resistance than Pd$_{black}$-50Pd/Al$_2$O$_3$, it may enable a long retention time for protons near the surface to promote complete hydrogenation, even at similar conversion and constant flow rate for both materials. With the higher flux of electrons resulting from higher current density (50 mA/cm^2), the Pd$_{black}$-50Pd/Al$_2$O$_3$ cathode could utilize more of its active sites to exhibit similar trends to that of Pd$_{black}$-5Pd/Al$_2$O$_3$. Comparing these cathodes, the key condition to improve selectivity for complete hydrogenation at the same total production rate is a balance of having a high charge transfer resistance that retains
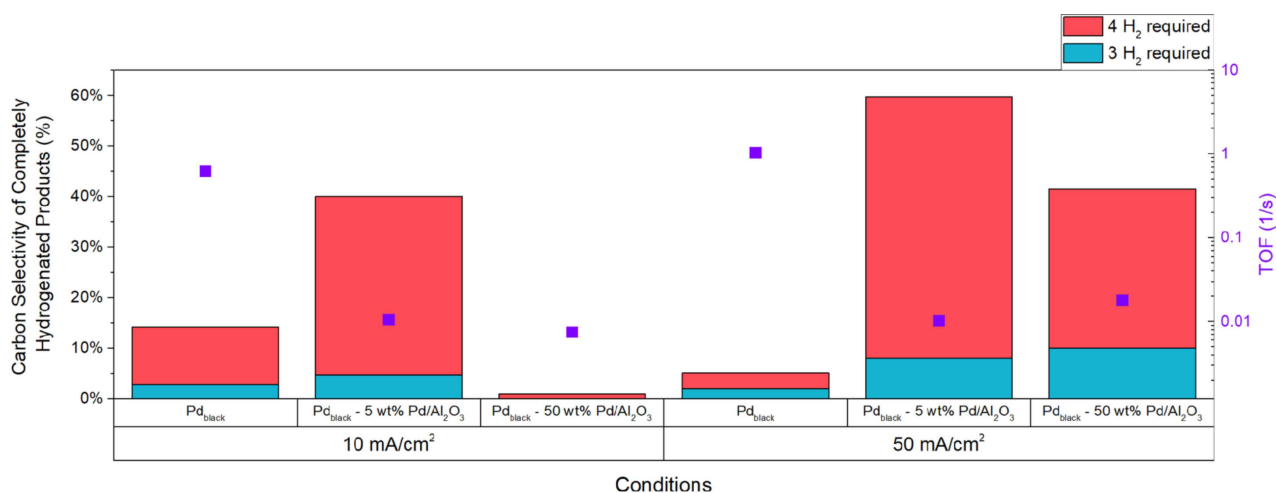
Figure 5. Carbon selectivities (left y-axis) of methyltetrahydrofuran (red) and tetrahydrofurfuryl alcohol (blue) and the log of turnover frequencies (right y-axis) for Pd_{black} and Pd_{black}-5Pd/Al$_2$O$_3$ at 10 mA/cm^2 (left three bars) and 50 mA/cm^2 (right three bars).

the molecules on the surface and a high number of active sites to increase the hydrogen coverage for promoting hydrogenation.

3. Conclusions

By varying current density to control proton delivery, we investigated the performance of hybrid Pd/Al$_2$O$_3$ cathodes and their constituent materials in terms of hydrogenation mechanisms, kinetics, and faradaic efficiency using furfural as a probe molecule. The electrocatalyst Pd_{black} exhibited a high selectivity for the hydrodeoxygenation pathway, with increase in production rate when the current density increased from 10 mA/cm^2 to 50 mA/cm^2. While the production rate was higher at 50 mA/cm^2 than at 10 mA/cm^2 due to the increase in flux of protons, the inefficient usage of protons for hydrogenation led to lower sum faradaic efficiency for the carbonaceous species and a shift in selectivity away from MTHF because less protons remained on the surface.

To exploit hydrogen adsorption and generation of Pd_{black}, Pd/Al$_2$O$_3$ was mixed with the Pd_{black} to form a hybrid cathode that enhances selectivity towards hydrogenation. Adding insulating alumina lowered conductivity and performance of the Pd_{black}. When the same amount of Pd_{black} was utilized, the performance of the Pd_{black}-Al$_2$O$_3$ cathode was hindered by the reduction of proton conductivity across the whole surface during the reaction compared to that of Pd_{black} cathode. However, by loading Pd onto Al$_2$O$_3$, the hindering effect of the insulating material can be negated at varying degrees. The cathode with low Pd loading, Pd_{black}-2.7Pd/Al$_2$O$_3$, exhibited similar unstable behavior to that of Pd_{black}-Al$_2$O$_3$. In contrast, Pd_{black}-50Pd/Al$_2$O$_3$ demonstrated more stable proton conductivity but suffered losses in rate, faradaic efficiency, and selectivity towards MTHF due to inefficient use of active material. The optimal Pd loading for the hybrid cathode tested was 5 wt% Pd/Al$_2$O$_3$. While Pd_{black}-5Pd/Al$_2$O$_3$ still suffered instability in

retaining constant production rate at 50 mA/cm^2, this cathode demonstrated similar production rates and faradaic efficiency as Pd_{black} at both current densities as well as selectivity towards the completely hydrogenated hydrodeoxygenation product.

Based on comparing Pd_{black} physically mixed with different loadings of Pd on Al$_2$O$_3$, the key factors for improving overall activity for hydrogenation were number of active sites and stable conductivity throughout the reaction. All Pd/Al$_2$O$_3$ cathodes have higher amount of electrochemical active sites than Pd_{black}, facilitating an increase in hydrogen coverage on the catalyst surface that can promote hydrogenation. However, the proton conductivity has to be stable throughout the reaction for efficient use of available active sites. Similarly, these Pd/Al$_2$O$_3$ containing cathodes have a higher charge transfer resistance than that of Pd_{black}, indicating that the electron transfer for any electrochemical reaction will be slower. The slower electron transfer for these hybrid cathodes can promote longer retention of the molecules (furfural, H$_2$, or intermediates) on the surface, enabling complete hydrogenation of furfural. These three factors were balanced for the Pd_{black}-5Pd/Al$_2$O$_3$, demonstrating that higher selectivity for complete hydrogenation is possible at similar rates as Pd_{black} due to the addition of 0.1 mg/cm^2 of Pd/Al$_2$O$_3$ that enhances stability and number of active sites. Further improvements for designing these hybrid cathodes for selective hydrogenations in electrochemical systems should focus on determining the best dispersion of the metal on the metal oxide and optimal particle size that can retain stability during reactions. Overall, these hybrid cathodes have demonstrated the potential to expand the design space of an electrocatalyst. Optimization of these hybrid cathodes can improve stability and fine-tune control over selectivity, both of which pose major limitations for electrocatalytic hydrogenation. With improved understanding of major influences on hybrid cathode design, the potential of electrocatalytic process can be expanded and explored to provide better control over selective hydrogenation compared to conventional thermocatalytic process. This improved control and ease of integration with renew-

able energy sources make electrochemical hydrogenation worthy of further investigation for increasing sustainability of industrial hydrogenation processes.

Acknowledgments

Conflict of Interest

The authors declare no conflict of interest.

[1] P. Virtanen, E. Salminen, P. Mäki-Arvela, J.-P. Mikkola, *Supported Ionic Liquids: Fundamentals and Applications, 1st Ed.*, (Eds.: R. Fehrmann, A. Riisager, M. Haumann), Wiley-VCH, **2014**, 251–262.
[2] R. M. Machado, K. R. Heier, R. R. Broekhuis, *Curr. Opin. Drug Discov. Devel.* **2001**, *4*, 745–755.
[3] K. R. Westerterp, E. J. Molga, K. B. van Gelder, *Chem. Eng. Process.* **1997**, *36*, 17–27.
[4] W. Bonrath, J. Medlock, J. Schütz, B. Wüstenberg, T. Netscher, *Hydrogenation*, (Ed.: I. Karamé) **2012**, 69–90.
[5] A. Garron, W. A. Maksoud, C. Larabi, P. Arquillière, K. C. Szeto, J.-J. Walter, C. C. Santini, *Catal. Today* **2014**, *255*, 75–79.
[6] *Fundamentals of Industrial Catalytic Processes, 2nd ed.*, (Eds.: R. J. Farrauto, C. H. Bartholomew) John Wiley & Sons, Inc., **2006**, 1–970.
[7] M. Rojas, S. Zeppieri, *Catal. Today* **2014**, *220–222*, 237–247.
[8] M. Vilar, J. L. Oliveira, M. Navarro, *Appl. Catal. A* **2010**, *372*, 1–7.
[9] R. Fonocho, C. L. Gardner, M. Ternan, *Electrochim. Acta* **2012**, *75*, 171–178.
[10] M. J. Orella, Y. Román-Leshkov, F. R. Brushett, *Curr. Opin. Chem. Eng.* **2018**, *20*, 159–167.
[11] X. H. Chadderdon, D. J. Chadderdon, J. E. Matthiesen, Y. Qiu, J. M. Carraher, J.-P. Tessonier, W. Li, *J. Am. Chem. Soc.* **2017**, *139*, 14120–14128.
[12] J. Lessard, *Organic Electrochemistry, 5th Ed.*, (Eds.: O. Hammerich, B. Speiser), CRC Press, **2015**, 1657–1671.
[13] H. Vogt, G. Kreysa, S. Vasudevan, R. Wüthrich, J. D. A. Ziki, R. El-Haddad, *Ullmann's Encyclopedia of Industrial Chemistry*, Wiley-VCH, **2013**, 1–49.
[14] A. H. Sulaymon, A. H. Abbar, *Electrolysis* **2012**, 189–202.
[15] P. Trinidad, F. Walsh, D. Gilroy, *Int. J. Eng. Educ.* **1998**, *14*, 431–441.
[16] S. Sen, D. Liu, G. T. R. Palmore, *ACS Catal.* **2014**, *4*, 3091–3095.
[17] E. J. Horn, B. R. Rosen, P. S. Baran, *ACS Cent. Sci.* **2016**, *2*, 302–308.
[18] W. An, J. K. Hong, P. N. Pintauro, K. Warner, W. Neff, *J. Am. Oil Chem. Soc.* **1999**, *75*, 917–925.
[19] P. N. Pintauro, *Hydrogenation of Fats and Oils: Theory and Practice, 2nd Ed.*, (Eds.: G. R. List, J. W. King), AOCS Press **2010**, 279–304.
[20] K. Scott, *Asia-Pacific J. Chem.* **1993**, *1*, 71–117.
[21] G. G. Botte, *Electrochem. Soc. Interface* **2014**, *23*, 49–55.
[22] C. Liu, A.-Y. Zhang, D.-N. Pei, H.-Q. Yu, *Environ. Sci. Technol.* **2016**, *50*, 5234–5242.
[23] S. K. Green, J. Lee, H. J. Kim, G. A. Tompsett, W. Bae, G. W. Huber, *Green Chem.* **2013**, *15*, 1869–1879.
[24] S. K. Green, G. A. Tompsett, H. J. Kim, W. B. Kim, G. W. Huber, *ChemSusChem* **2012**, *5*, 2410–2420.
[25] Y. Song, U. Sanyal, D. Pangotra, J. D. Holladay, D. M. Camaioni, O. Y. Gutiérrez, J. A. Lercher, *J. Catal.* **2018**, *359*, 68–75.

[26] A. Sáez, V. García-García, J. Solla-Gullón, A. Aldaz, V. Montiel, *Electrochim. Acta* **2013**, *91*, 69–74.
[27] R. Kas, R. Kortlever, A. Milbrat, M. T. M. Koper, G. Mul, J. Baltrusaitis, *Phys. Chem. Chem. Phys.* **2014**, *16*, 12194–12201.
[28] K. P. Kuhl, E. R. Cave, D. N. Abram, T. F. Jaramillo, *Energy Environ. Sci.* **2012**, *5*, 7050–7059.
[29] K. Takano, H. Tateno, Y. Matsumura, A. Fukazawa, T. Kashiwagi, K. Nakabayashi, K. Nagasawa, S. Mitsushima, M. Atobe, *Bull. Chem. Soc. Jpn.* **2016**, *89*, 1178–1183.
[30] U. S. Energy Information Administration **2018**. [Online]. Available: https://www.eia.gov/energyexplained/?page=us_energy_home#tab1. [Accessed: 20-Aug-2018].
[31] U. S. Energy Information Administration, *Mon. Energy Rev.* **2018**, *185*.
[32] Z. Qi, *Proton Exchange Membrane Fuel Cells*, CRC Press **2014**, 1–371.
[33] H. Chhina, S. Campbell, O. Kesler, *J. Power Sources* **2007**, *164*, 431–440.
[34] S. J. Paddison, H. A. Gasteiger, *Encyclopedia of Sustainability Science and Technology*, (Ed.: R. A. Meyers), Springer, **2013**, 8347–8372.
[35] J. C. Meier, C. Galeano, I. Katsounaros, J. Witte, H. J. Bongard, A. A. Topalov, C. Baldizzone, S. Mezzavilla, F. Schüth, K. J. J. Mayrhofer, *Beilstein J. Nanotechnol.* **2014**, *5*, 44–67.
[36] F. M. Sapountzi, J. M. Gracia, C. J. Weststrate, H. O. A. Fredriksson, J. W. Niemantsverdriet, *Prog. Energy Combust. Sci.* **2017**, *58*, 1–35.
[37] N.-T. Suen, S.-F. Hung, Q. Quan, N. Zhang, Y.-J. Xu, H. M. Chen, *Chem. Soc. Rev.* **2017**, *46*, 337–365.
[38] G. J. K. Acres, J. C. Frost, G. A. Hards, R. J. Potter, T. R. Ralph, D. Thompsett, G. T. Burstein, G. J. Hutchings, *Catal. Today* **1997**, *38*, 393–400.
[39] B. G. Pollet, A. A. Franco, H. Su, H. Liang, S. Pasupathi, *Compendium of Hydrogen Energy*, (Eds.: F. Barbir, A. Basile, T. N. Veziroğlu), Elsevier Ltd., **2016**, *3*, 3–56.
[40] A. C. Lausche, K. Okada, L. T. Thompson, *Electrochem. Commun.* **2012**, *15*, 46–49.
[41] S. Sitthisa, D. E. Resasco, *Catal. Lett.* **2011**, *141*, 784–791.
[42] R. Mariscal, P. Maireles-Torres, M. Ojeda, I. Sádaba, M. López Granados, *Energy Environ. Sci.* **2016**, *9*, 1144–1189.
[43] S. Wang, V. Vorotnikov, D. G. Vlachos, *ACS Catal.* **2015**, *5*, 104–112.
[44] B. B. Baker, *Am. Ind. Hyg. Assoc. J.* **1974**, *35*, 735–740.
[45] Y. Yang, J. Ma, X. Jia, Z. Du, Y. Duan, J. Xu, *RSC Adv.* **2016**, *6*, 51221–51228.
[46] S. H. Pang, J. W. Medlin, *ACS Catal.* **2011**, *1*, 1272–1283.
[47] M. Lesiak, M. Binczarski, S. Karski, W. Maniukiewicz, J. Rogowski, E. Szubiakiewicz, J. Berlowska, P. Dziugan, I. Witońska, *J. Mol. Catal. A* **2014**, *395*, 337–348.
[48] L. Liu, W. Zhang, W. Huang, Y. He, L. Liu, C. Wang, H. Lin, *J. Electroanal. Chem.* **2017**, *804*, 248–253.
[49] N. S. Date, N. S. Biradar, R. C. Chikate, C. V. Rode, *ChemistrySelect* **2017**, *2*, 24–32.
[50] P. Nilges, U. Schröder, *Energy Environ. Sci.* **2013**, *6*, 2925.
[51] S. Bhogeswararao, D. Srinivas, *J. Catal.* **2015**, *327*, 65–77.
[52] V. Vorotnikov, G. Mpourmpakis, D. G. Vlachos, *ACS Catal.* **2012**, *2*, 2496–2504.
[53] H. Guo, H. Zhang, L. Zhang, C. Wang, F. Peng, Q. Huang, L. Xiong, C. Huang, X. Ouyang, X. Chen, X. Qiu, *Ind. Eng. Chem. Res.* **2018**, *57*, 498–511.
[54] L. J. Liu, H. M. Guo, B. Xue, H. Lou, M. Chen, *RSC Adv.* **2015**, *5*, 66704–66710.
[55] Y. Shi, Y. Zhu, Y. Yang, Y. W. Li, H. Jiao, *ACS Catal.* **2015**, *5*, 4020–4032.
[56] *PEM Fuel Cell Electrocatalysts and Catalyst Layers: Fundamentals and Applications*, (Ed: J. Zhang), Springer-Verlag London Limited, **2008**, 1–1137.
[57] B. D. Adams, A. Chen, *Mater. Today* **2011**, *14*, 282–289.
[58] H. Dropsch, M. Baerns, *Appl. Catal. A* **1997**, *158*, 163–183.
[59] K. Murata, Y. Mahara, J. Ohyama, Y. Yamamoto, S. Arai, A. Satsuma, *Angew. Chem. Int. Ed.* **2017**, *56*, 15993–15997; *Angew. Chem.* **2017**, *129*, 16209–16213.
[60] A. Redjel, A.-G. Boudjahem, M. Bettahar, *Part. Sci. Technol.* **2018**, *36*, 710–715.